Pol. J. Environ. Stud. Vol. 30, No. 5 (2021), 4579-4585
DOI: *10.15244/pjoes/130975* ONLINE PUBLICATION DATE: 2021-08-16

Original Research

Highly Selective and Efficient Porous Cu-Sn Bimetallic Electrocatalyst for CO_2 Reduction to Formate

Rana Rashad Mahmood Khan[1], Ramsha Saleem[1], Rashida Bashir[2], Muhammad Pervaiz[1], Sadaf Naz[3], Shafiq Ur Rehman[4], Umer Younas[3], Shan e Batool[3] Hafiz Muhammad Faizan Haider[1], Munawar Iqbal[3], Ahmad Adnan[1,*]

[1]Department of Chemistry, Government College University, Lahore, Pakistan
[2]Department of Chemistry, University of Education, Lahore, Pakistan
[3]Department of Chemistry, The University of Lahore, Lahore, Pakistan
[4]Department of Chemistry, University of Central Punjab, Lahore, Pakistan

Received: 8 July 2020
Accepted: 28 November 2020

Abstract

In the current study, a simple chemical reduction method to synthesize bimetallic nanocatalyst of $CuSn(OH)_6$ has been reported. The morphology, composition, size and electrochemical activity of the nanocatalyst have been investigated. The nanocatalyst exhibits porous/sponge-like morphology. The linear sweep voltammetry and chronoamperometry were employed to measure the current density/current response. The synthesized catalyst was used for electrochemical reduction of CO_2 to formate. The electrocatalytic results confirmed higher faradaic efficiency (FE), high and long term stable current density and lower Tafel slope for the synthesized nanocatalyst. The maximum obtained FE on bimetallic electrocatalyst for the only liquid product (formate) was nearly 83%. The improved electrocatalytic activity confirms synergistic effect between Cu and Sn as nanocatalyst that efficiently contributed towards the conversion of CO_2 to formate. Therefore, $CuSn(OH)_6$ nanocatalyst can be prepared by a simple and cost-effective method that can be further used for efficient and selective reduction of CO_2.

Keywords: bimetallic nanoparticles, CO_2 reduction, electrocatalyst, formate, porous catalyst, Faradaic efficiency

Introduction

Carbon dioxide (CO_2) is a ubiquitous and necessary molecule to sustain life on Earth. The concentration of CO_2 in the atmosphere is increasing day by day due to the burning of fossil fuels for industries and human activities [1]. The concentration of CO_2 in the atmosphere has surpassed the level of 400 ppm in human history [2-4]. Such massive emission of CO_2 in the atmosphere has caused air pollution and the greenhouse effect [5, 6]. To rectify the adverse effects of atmospheric CO_2 and to reduce its level, several methods

*e-mail:ahmadadnan@gcu.edu.pk

such as chemical reduction, electrochemical reduction, and photochemical reduction are usually employed. Reports revealed that electrochemical reduction is best among all the techniques, as it is eco-friendly and easy to establish [7-9]. Being linear molecule, CO_2 molecule is thermodynamically stable [10-12] having high activation overpotential that results in slow reaction kinetics [11, 13, 14] for its reduction reaction. The $1e^-$ reduction of CO_2 to $CO_2^{\bullet-}$ requires high overpotential i.e. $E°$ = -1.90 V *vs* Standard Hydrogen Electrode at pH 7 [15]. This high overpotential may be due to the change in geometry of CO_2 from a linear molecule to a bent molecule [16]. In addition, low faradaic efficiency (FE), poor product selectivity [17], and competitive side reaction like hydrogen evolution reaction significantly lowers the CO_2 reduction products [13, 18].

Electroreduction of CO_2 may yield variety of products and formate is one of the organic molecules produced during CO_2 reduction [19, 20]. Formate is a simple, stable, nontoxic liquid and natural organic molecule [11, 21] that is used in dyes, leather, pesticides, silicones, and pharmaceutical industries. It is also used for the protection of crops, deicing of craft, in fuel cell and as an intermediate in many chemical processes [5, 11]. In order to convert CO_2 to formate at low activation overpotential with high FE, an efficient, stable and product selective electrocatalyst is still needed.

Catalyst and electrode material contributes significantly to determining the overpotential, FE, and nature of the product in CO_2 reduction [22, 23]. Hori et al. reported that Pb, In, Cd, Tl, Bi, and Sn have been reported as efficient catalyst for formate production but require high negative potential [24-27] while Cu is famous for hydrocarbons [13, 28]. Some of the tested metals (Pb, Hg, Cd, In) are not preferred due to high cost and toxicity issues [29]. Copper expresses excellent behavior for electrochemical conversion of CO_2 to a variety of chemicals, but its selectivity is low [30]. However, Sn-based catalysts are good candidates for formate production because they are cost effective, selective and ecofriendly [11, 31, 32]. The catalytic activity and product selectivity can be improved by changing the catalyst or by changing the morphology of the catalyst after alloying [13, 33-35]. Therefore, the selectivity of Cu catalysts can be enhanced by the incorporation of secondary metal especially Sn, In, Ag and Al [30].

In this manuscript, the preparation of Cu-Sn bimetallic nanocatalyst and their catalytic activity has been presented. The Cu-Sn bimetallic nanocatalyst was prepared by the chemical reduction method, which is cost-effective, time-saving and superficial. Synthesized alloy nanocatalyst was investigated for their catalytic activities for the conversion of CO_2 to formate. Electrochemical study confirmed excellent stability, activity, current density, FE and formate selectivity. In addition, problems of product selectivity, high overpotential, low stability, current density and FE have been addressed successfully.

Material and Methods

Chemicals and Reagents

Salts of copper (II) chloride dihydrate ($CuCl_2.2H_2O$), sodium dodecyl sulfate ($NaC_{12}H_{25}SO_4$), and tin(II) chloride dihydrate ($SnCl_2.2H_2O$) and Isopropyl alcohol (IPA, C_3H_8O) were purchased from Unichem (China). The sodium borohydride ($NaBH_4$, ≥96%,) was obtained from Sigma Aldrich. Food grade carbon dioxide (CO_2, 99.999%) was obtained from the local market.

Preparation of $CuSn(OH)_6$ Catalyst

The nanocatalyst of copper-tin hydroxide ($CuSn(OH)_6$) were prepared via the chemical reduction method. $CuCl_2.2H_2O$ and $SnCl_2.2H_2O$ were used as precursor salts. First, the weighed amount of 0.86 g $CuCl_2.2H_2O$ and 4.06 g $NaC_{12}H_{25}SO_4$ were dissolved in 50 mL of distilled water and then 50 mL of IPA was added. The prepared mixture was then shifted to a 250 mL three neck round bottom (RB) flask. The RB flask was placed in a water bath at 50ºC under a constant stirring of 500 rpm for 1 h. Then 10 mL of 5 M aqueous $NaBH_4$ was added dropwise. After 20 min, 0.101 g of $SnCl_2.2H_2O$ was added in the above mixture and heated for 3 h. The stirring and temperature of the reaction contents were maintained throughout the experiment. Synthesized nanocatalyst was collected through centrifugation (4000 rpm) for half an hour and then washed many times with water to remove the surfactant or any other water-soluble impurity. After washing, the final product was then dried in an oven at 70ºC for 24 h and calcined at 300ºC for 1 h.

Catalyst Characterization

The suspension of nanocatalyst was prepared in IPA through ultra-sonification for particle size analysis and UV- Visible spectroscopy. The size of the nanocatalyst was estimated with particle size analyzer based on the dynamic light scattering (DLS) technique. The absorption spectrum, λ_{max}, and energy bandgap were calculated from UV-Visible spectroscopy data. X-ray diffraction (XRD) pattern was acquired with Cu-Kα radiations (λ = 1.54059 Å, scan range 15-60° with step 0.05, scan rate 0.5 degree/min) and used to verify the crystal structure of the sample with JCPDS powder diffraction database. The percent crystallinity, the lattice constant, and hkl value were calculated from XRD data. The crystallite size was calculated employing Debye Scherrer's equation. Scanning electron microscope (SEM) images were taken to observe the morphology of the nanocatalyst. The fluorine-doped tin oxide (FTO) substrate was coated with catalyst ink/ slurry (detail of ink formation and catalyst coating are given in the electrode fabrication) to get SEM images. The FTO substrates adhered to the sample holder with conductive double-sided carbon tape. Linear

sweep voltammetry (LSV) and chronoamperometry (CA) were finalized to evaluate the electrocatalytic behavior (current density) and stability of the catalyst for CO_2RR.

Electrode Fabrication

The working electrode was prepared on the FTO substrate (a conducting glass) with a dimension of 1×2 cm^2. First, the FTO was dipped in 20 mL of ethanolic saturated KOH at 60ºC and the 1 A current was passed for 2 min to activate the substrate, then washed with deionized water and air-dried. The ink/slurry of the catalyst was prepared by taking 10 mg of $CuSn(OH)_6$ catalyst in 950 µL of IPA and 50 µl of 5 %wt Nafion solution and subjected to ultrasonication for 3 h. Then the 50 µL slurry was drop cast on the activated FTO substrate and left for overnight drying at ambient conditions. After drying it was used for the electrocatalytic measurements.

Electrocatalysis Evaluation

The Metrohm auto lab (BV PGSTAT302N) with a three-electrode system was used for the electrochemical measurements. The two electrode compartments (H type cell) were separated with proton exchange membrane Nafion NRE-212 Sigma Aldrich. This separation helps to prevent the re-oxidation of reduction products of CO_2. The 0.1 M $KHCO_3$ was used as an electrolyte. The 35 mL of electrolyte was filled in each compartment (cathodic and anodic). The catholyte was fed and saturated with CO_2 for at least 1 h before the start of electroreduction. The FTO substrate, coated with catalyst was inserted into the cathodic compartment as a working electrode. The Ag/AgCl electrode, a reference electrode, was positioned in the catholyte with proximity to the working electrode and the Pt sheet, the counter electrode, was inserted in the anolyte. The LSV (potential window from 0 to -1V, scan rate of 50 mV/s) and CA (at a fixed voltage of 0.9 V for 9) were performed to measure the response of current. All the reported potentials are against Ag/AgCl electrode otherwise stated. The reduction current and concentration of products were used to measure the catalytic activity.

Results and Discussion

Characterization of Nanocatalyst

The UV spectrum was measured from 250 to 800 nm to evaluate the optical properties of the catalyst and the result is shown in Fig. 1. The UV spectrum shows a single absorption peak at 293 nm. The Cu_xO_y shows the maximum absorption at 258 nm and ~650 nm while the pure copper nanoparticles have been reported to exhibit maximum absorption at 570-582 nm [36, 37].

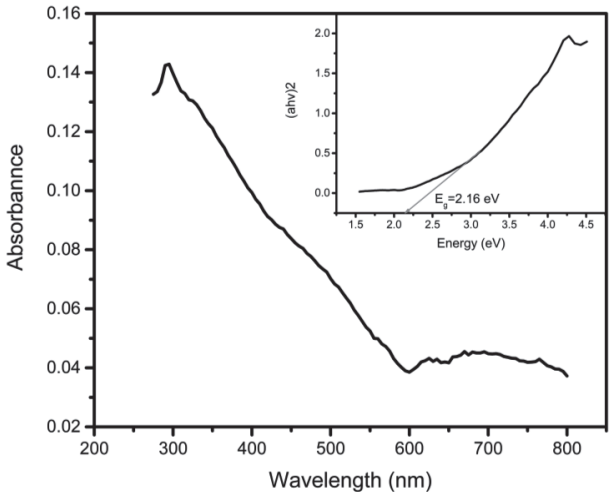

Fig. 1. UV-visible absorption spectra of $CuSn(OH)_6$ (Inset Tauc plot).

The absorption maxima for SnO and Sn/SnO_{2-x} were reported in the range of 310-325 nm and 520-530 nm respectively [38]. The absence of characteristic peaks of Cu_xO_y, Cu, Sn, and Sn/SnO_{2-x} rule out the presence of these individual nanoparticles. The absorption peak present in the IR region is at a lower wavelength from the nanoparticles cited in the literature, which indicates the nanocatalyst has blue-shifted and gives a strong response to the shorter wavelength that indicate smaller particle size of the nanocatalyst.

Dynamic light scattering (DLS) is a fast and easy technique for particle size distribution and to estimate the average size of the nanocatalyst [39]. We measured the average particle size by using particle size analyzer and the outcome is shown below in Fig. 2. The average estimated size of the nanocatalyst particles was found in the range of 10-22 nm. According to the literature, increase in catalytic activity may be observed due to smaller particle size as the surface area increases, as the size decreases. Thus, our catalyst may be efficient and highly active for CO_2 reduction. The presence of a sharp peak indicates the nanocatalyst is monodispersed and of good quality.

The surface morphology of the catalyst was characterized by using SEM at different resolutions i.e. 2 and 5 µm. Fig. 3 shows the surface of catalysts is sponge-like and porous with interconnected pores. The catalyst with a sponge-like morphology is beneficial and efficient because it provides high surface area which helps in the transportation of metal solvated ions as well as the maximum availability of the active sites of the catalyst. Moreover, the porous structure helps the electrochemical reduction of CO_2 by suppressing the hydrogen evolution reaction [40].

Powder X-Ray diffraction was used to check the crystalline structure, material composition, size of the crystallite and percent crystallinity. Fig. 4 presents the XRD pattern and unveils the highly crystalline nature (84%) of the as-prepared $CuSn(OH)_6$ catalyst.

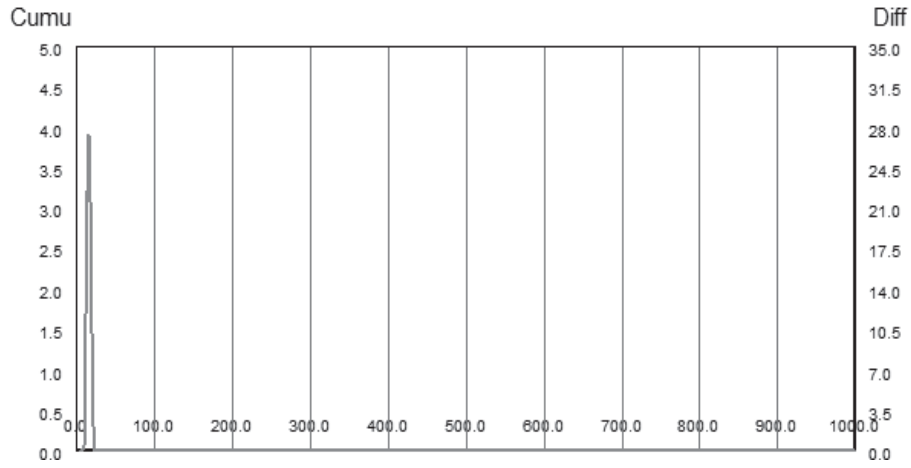

Diam nm	Percent
8.89	0.00
9.84	0.41
10.9	3.45
12.0	11.75
13.3	28.04
14.8	50.70
16.4	72.71
18.1	89.39
20.1	97.98
22.3	100.00

Fig. 2. Average size distribution of $CuSn(OH)_6$ nanocatalyst.

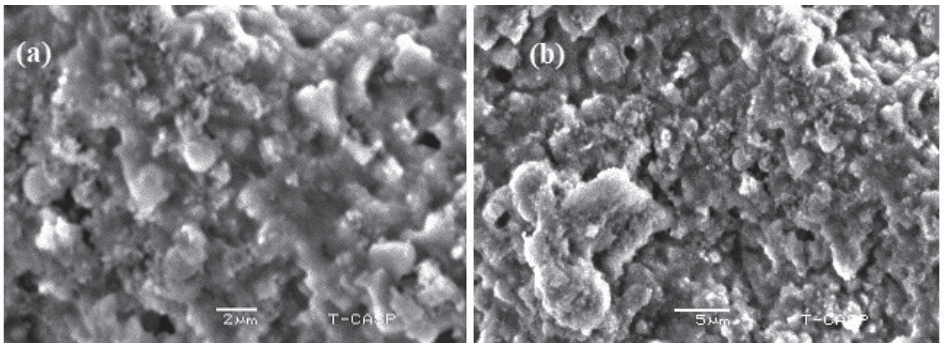

Fig. 3. SEM images of $CuSn(OH)_6$ at different resolutions a) 2 µm b) 5 µm.

The diffraction peaks in the XRD pattern denotes the Bragg's reflections. The diffraction peaks at various positions (2θ) value 18.76°, 22.56°, 31.94°, 35.56°, 37.81°, 39.52°, 42.29°, 46.24°, 52.65°, and 58.19° correspond to the (111), (200), (220), (310), (311), (222), (321), (400), (420), (422) planes/facet of the crystalline phase. This crystalline phase is following JCPDS# 00-038-0394 (Crystal system: Cubic, a: 7.7350Å, Space group: Pn-3 m, Space group number: 224). The Debye Scherrer's equation was used to calculate the average crystallite size that was found in the range 16-22 nm. The particle size obtained from XRD is in agreement with the size obtained from DLS.

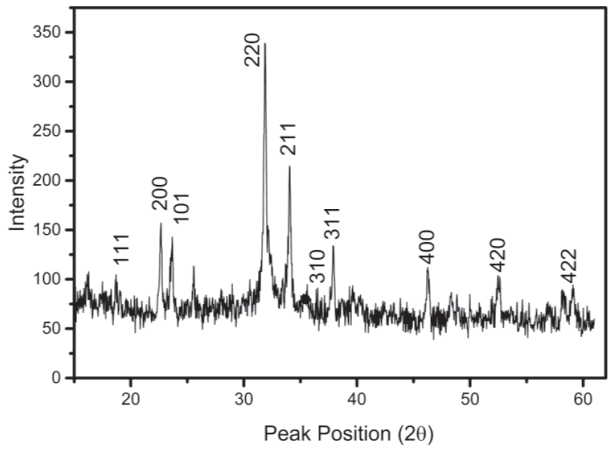

Fig. 4. P-XRD pattern of $CuSn(OH)_6$

Electrochemical Performance

For electrochemical measurements of the catalyst, the H type cell was used. Fig. 5a) shows the LSV curves for the $CuSn(OH)_6$ catalyst in CO_2 saturated electrolyte (black) and air (grey). The onset potential and onset overpotential were calculated from the LSV curve and found to be -428 mV and -660 mV *vs* Ag/AgCl respectively. The catalyst with large onset overpotential (-660 mV) suppresses the HER that is the distinctive feature of the catalyst and is in agreement with its porous morphology. The suppression in HER favors the CO_2RR otherwise current is consumed in HER instead of CO_2 reduction. This indicates our catalyst is more specific for CO_2RR. A continuous increase in current density was observed beyond the onset potential. The maximum obtained current density was 24 mA/cm^2 at -1 V. The large current density is also compatible with the surface morphology of the catalyst. The small size

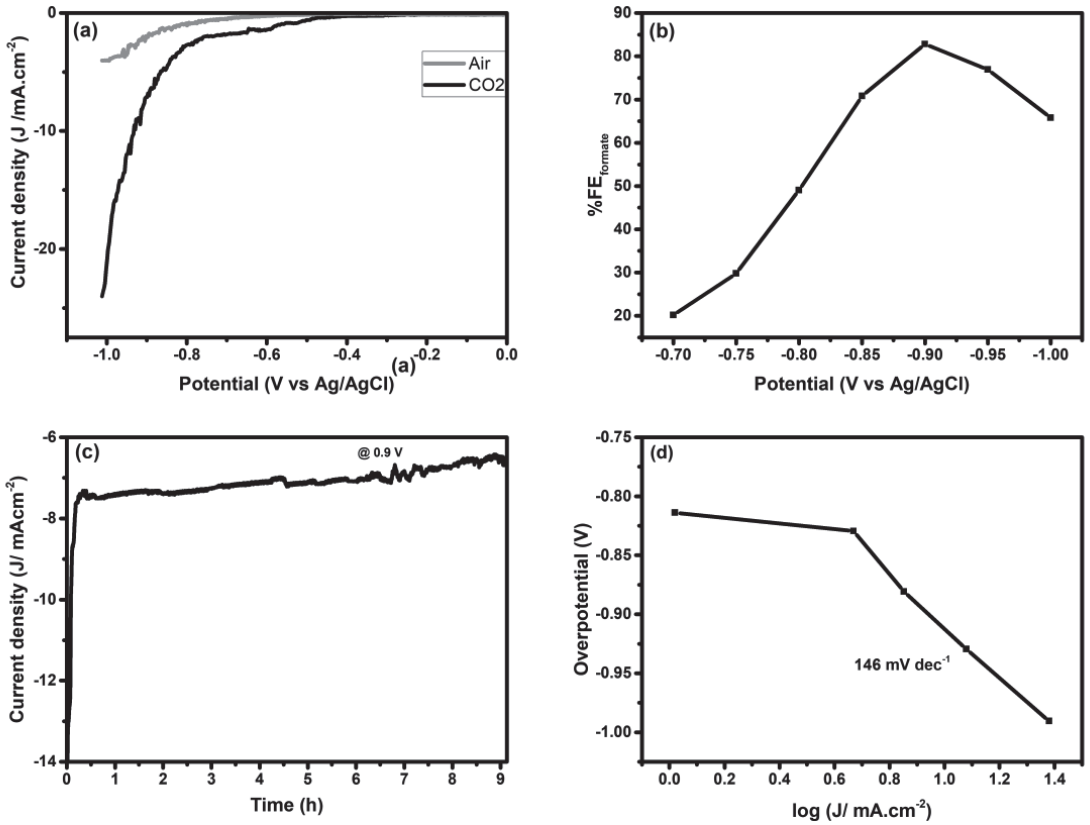

Fig. 5. a) LSV curve for CO_2 saturated electrolyte (black) and without CO_2 saturation (red). b) % FE for formate at different potentials c) Current response in chronoamperometry at 0.9 V vs Ag/AgCl d) Tafel plot for the formation of formate in 0.1M $KHCO_3$

and the porous structure of the catalyst provide high surface area with a large number of active sites, which in turn improves the catalytic efficiency. The onset potential for air was high and the current density was lower as compared to the CO_2 saturated electrolyte. The increase in current density in CO_2 saturated electrolyte indicates the high activity of the catalyst for CO_2RR.

The CO_2 electroreduction at different potentials (-0.7 to -1.0 V) was executed for the identification, quantification/characterization of products. Ion chromatography (Akta pure M1 model of FPLC equipped with ion exchange column) and UV visible spectroscopy was used for the identification and quantification of liquid product.

The electrocatalytic reduction of CO_2 was accomplished for 1 h at each potential (-0.7 to -1.0 V) for the product identification and FE calculation. The electrolyte sample was analyzed and results showed that the only liquid product under all potentials from CO_2 reduction was formate. The FEs for formate as a function of the potential is represented in Fig. 5b). A climb is observed in the $FE_{Formate}$ with the increase in applied potential from -0.75 to -0.9 V. The maximum obtained FE was 82.8% at -0.9 V and a decrease in FE is observed beyond this potential. The highest FE for formate represents the collaboration between two metals and the presence of Cu with Sn modified the features of electroactive species.

For stability test, CA was done at -0.9 V for 9 h in CO_2 saturated electrolyte. Fig. 5c) shows the stable cathodic current density during the chronoamperometric analysis which evidences the constancy of the catalyst. During bulk analysis, the average obtained $FE_{formate}$ was 78% which represents the high activity of the catalyst for long-term electrocatalysis. The stability test proves that the pre-synthesized $CuSn(OH)_6$ acts as a robust electrode and can be used in any device to reduce waste CO_2 into formate.

The Tafel slope helps in the understanding of reaction kinetics/mechanism. The small value of the Tafel slope represents the high catalytic efficiency and the lower rate-limiting activation energy barrier. The Tafel plot was constructed to gain kinetic insights and the reaction pathway for CO_2 electroreduction to formate in the applied potential range of -0.7 to -1 V Fig. 5d). The obtained Tafel slope value (146 mV/dec) is following the mechanistic hypothesis which denotes the rate-determining step is the transfer of the first electron to the surface adsorbed CO_2 for the formation of radical anion ($CO_2^{\cdot-}$) intermediate [41, 42]. Along with the reaction mechanism, the small slope also suggests that $CuSn(OH)_6$ exhibits the high reaction kinetics for CO_2 reaction.

The electrocatalytic activity, stability, and product selectivity of the catalyst was efficient and comparable with the literature i.e. hierarchical porous Cu foam

at -1 V vs Ag/AgCl) [43] fibrous Cu at -1.1 V vs Ag/AgCl [44], porous SnO_2 wires at -0.8 V vs RHE [45], and 3D Sn foam on Sn film at -1.3 V vs RHE [46] have reduced CO_2 to formate with the FE of 43, 29, 80, and 90 % respectively. The selectivity, durability and electrocatalytic performance of the bimetallic catalyst for formate production were excellent.

Conclusions

The nanocatalyst $CuSn(OH)_6$ was successfully synthesized by a chemical reduction method for the electrochemical reduction of CO_2 to formate. The catalyst exhibits the high FE of 82.8% at 0.9 V vs Ag/AgCl with stable current density (~7.6 mA cm^{-2}) for 9 hours. The Tafel slope was only 146 mV/dec. The bimetallic catalyst exhibits admirable electrocatalytic activity towards CO_2RR to formate in aqueous electrolyte. The great combination of high current density, stability, high FE and product selectivity makes the catalyst highly effective and efficient for CO_2RR production from CO_2.

Conflict of Interest

The authors declare no conflict of interest.

References

1. LACIS A.A., SCHMIDT G.A., RIND D., RUEDY R.A. Atmospheric CO_2: Principal control knob governing Earth's temperature. Science, **330**, 356, **2010**.
2. NIELSEN D.U., HU X.M., DAASBJERG K., SKRYDSTRUP T. Chemically and electrochemically catalysed conversion of CO_2 to CO with follow-up utilization to value-added chemicals. Nat. Catal. **1**, 244, **2018**.
3. EWALD J. Carbon Dioxide at NOAA's Mauna Loa Observatory reaches new milestone: Tops 400 ppm. NOAA Res. **10**, **2013**.
4. NATAWIJAYA M.A., SUGAI Y., ANGGARA F. Technology P: CO_2 microbubble colloidal gas aphrons for EOR application: the generation using porous filter, diameter size analysis and gas blocking impact on sweep efficiency. J. Petrol. Explor. Prod. Technol. **10**, 103, **2020**.
5. PAWAR A.U., KIM C.W., NGUYEN-LE M.T., KANG YS. General Review on the Components and Parameters of Photoelectrochemical System for CO_2 Reduction with in Situ Analysis. ACS Sustainable Chem. Eng. **7**, 7431, **2019**.
6. YI Y., LU W., HONG D., LIU H., ZHANG L. Application of dual-response surface methodology and radial basis function artificial neural network on surrogate model of the groundwater flow numerical simulation. Pol. J. Environ. Stud. **26**, 1835, **2017**.
7. ASADI M., KUMAR B., BEHRANGINIA A., ROSEN B.A., BASKIN A., REPNIN N., PISASALE D., PHILLIPS P., ZHU W., HAASCH R. Robust carbon dioxide reduction on molybdenum disulphide edges. Nat. Commun. **5**,1, **2014**.
8. FRANCKE R., SCHILLE B., ROEMELT M. Homogeneously catalyzed electroreduction of carbon dioxide methods, mechanisms, and catalysts. Chem. Rev. **118**, 4631, **2018**.
9. DETWEILER Z.M., WHITE J.L., BERNASEK S.L., BOCARSLY A. Anodized indium metal electrodes for enhanced carbon dioxide reduction in aqueous electrolyte. Langmuir, **30**, 7593, **2014**.
10. CHRISTOPHE J., DONEUX T., BUESS-HERMAN C. Electroreduction of carbon dioxide on copper-based electrodes: activity of copper single crystals and copper–gold alloys. Electrocatalysis, **3**,139, **2012**.
11. WEN G., LEE D.U., REN B., HASSAN F.M., JIANG G., CANO Z.P., GOSTICK J., CROISET E., BAI Z., YANG L. Orbital interactions in bi-sn bimetallic electrocatalysts for highly selective electrochemical CO_2 reduction toward formate production. Adv. Energy Mater. **8**, **2018**.
12. CHOJNICKI B.H., MICHALAK M., ACOSTA M., JUSZCZAK R., AUGUSTIN J., DRÖSLER M., OLEJNIK J. Measurements of carbon dioxide fluxes by chamber method at the Rzecin wetland ecosystem, Poland. Pol. J. Environ. Stud. **19**, 283, **2010**.
13. KIM D., RESASCO J., YU Y., ASIRI A.M., YANG P. Synergistic geometric and electronic effects for electrochemical reduction of carbon dioxide using gold-copper bimetallic nanoparticles. Nat. Commun. **5**, 1, **2014**.
14. LEI Z., JIHAO C., ZHANG L., XIANGLING S., YONGHUI L., MIN F. Preparing Mn-CoO-supported pyrolysis coke catalyst with plasma and its application in the SCO denitration process. Pol. J. Environ. Stud. **28**, 3323, **2019**.
15. SCHNEIDER J., JIA H., MUCKERMAN J.T., FUJITA E. Thermodynamics and kinetics of CO_2, CO, and H^+ binding to the metal centre of CO_2 reduction catalysts. Chem. Soc. Rev. **41**, 2036, **2012**.
16. BENSON E.E., KUBIAK C.P., SATHRUM A.J., SMIEJA J.M. Electrocatalytic and homogeneous approaches to conversion of CO_2 to liquid fuels. Che. Soc. Rev. **38**, 89, **2009**.
17. KORTLEVER R., SHEN J., SCHOUTEN K.J.P., CALLE-VALLEJO F., KOPER M. Catalysts and reaction pathways for the electrochemical reduction of carbon dioxide. The J. Phys. Chem. Lett. **6**, 4073, **2015**.
18. LU Q,. JIAO F. Electrochemical CO_2 reduction: Electrocatalyst, reaction mechanism, and process engineering. Nano Energy, **29**, 439, **2016**.
19. ZHU C., WANG Q., WU C. Rapid and scalable synthesis of bismuth dendrites on copper mesh as a high-performance cathode for electroreduction of CO_2 to formate. J. CO_2 Util. **36**, 96, **2020**.
20. LASOCKI J., KOŁODZIEJCZYK K., MATUSZEWSKA A. Laboratory-scale investigation of biogas treatment by removal of hydrogen sulfide and carbon dioxide. P. J. Envron. Stud. **24**, 1427, **2015**.
21. WANG W.H., HIMEDA Y., MUCKERMAN J.T., MANBECK G.F., FUJITA E. CO_2 hydrogenation to formate and methanol as an alternative to photo-and electrochemical CO_2 reduction. Chem, Rev. **115**, 12936, **2015**.
22. HIRUNSIT P., SOODSAWANG W., LIMTRAKUL J. CO_2 electrochemical reduction to methane and methanol on copper-based alloys: theoretical insight. The J. Phys. Chem. C. **119**, 8238, **2015**.
23. GUO J., GUO P., YU M., SUN Z., LI P., YANG T., LIU J., ZHANG L. Chemical reduction of nitrate using nanoscale

bimetallic iron/copper particles. Pol. J. Environ. Stud. **27**, 2023, **2018**.
24. HORI Y., KIKUCHI K., SUZUKI S. Production of CO and CH_4 in electrochemical reduction of CO_2 at metal electrodes in aqueous hydrogencarbonate solution. Chem. Lett. **14**, 1695, **1985**.
25. HORI YI. Electrochemical CO_2 reduction on metal electrodes. Mod. Aspect. Electroc. 89, **2008**.
26. HORI Y., WAKEBE H., TSUKAMOTO T., KOGA O. Electrocatalytic process of CO selectivity in electrochemical reduction of CO_2 at metal electrodes in aqueous media. Electrochimica Acta, **39**, 1833, **1994**.
27. KORTLEVER R., PETERS I., KOPER S., KOPER M. Electrochemical CO_2 reduction to formic acid at low overpotential and with high faradaic efficiency on carbon-supported bimetallic Pd–Pt nanoparticles. ACS Catal. **5**, 3916, **2015**.
28. KORTLEVER R., TAN K., KWON Y., KOPER M. Electrochemical carbon dioxide and bicarbonate reduction on copper in weakly alkaline media. J. Solid State Electr. **17**, 1843, **2013**.
29. FU Y., WANG T., ZHENG W., LEI C., YANG B., CHEN J., LI Z., LEI L., YUAN C., HOU Y. Nanoconfined tin oxide within N-doped nanocarbon supported on electrochemically exfoliated graphene for efficient electroreduction of CO_2 to formate and C1 products. ACS Appl. Mater. Inter. **12**, 16178, **2020**.
30. ZENG J., BEJTKA K., JU W., CASTELLINO M., CHIODONI A., SACCO A., FARKHONDEHFAL M.A., HERNÁNDEZ S., RENTSCH D., BATTAGLIA C. Advanced Cu-Sn foam for selectively converting CO_2 to CO in aqueous solution. Appl. Catal. B-Environ. **236**, 475, **2018**.
31. SEN S., BROWN S.M., LEONARD M., BRUSHETT F.R. Electroreduction of carbon dioxide to formate at high current densities using tin and tin oxide gas diffusion electrodes. J. Appl. Electr. **49**, 917, **2019**.
32. GÜLLÜCE M., KARADAYI M., DEMIR A.Y., IŞIK C., ALAYLAR B., İSPIRLI N. Genotoxic potentials of biosynthesized zinc oxide nanoparticles. Pol. J. Environ. Stud. 29, 2020.
33. PETERSON A.A., NØRSKOV J. Activity descriptors for CO_2 electroreduction to methane on transition-metal catalysts. The J. Phys. Chem. Lett. **3**, 251, **2012**.
34. VALERIO-RODRÍGUEZ M.F., TREJO-TÉLLEZ L.I., AGUILAR-GONZÁLEZ M.Á., MEDINA-PÉREZ G., ZÚÑIGA-ENRÍQUEZ J.C., ORTEGÓN-PÉREZ A., FERNÁNDEZ-LUQUEÑO F. Effects of ZnO, TiO_2 or Fe_2O_3 nanoparticles on the body mass, reproduction, and survival of eisenia fetida. Pol. J. Eviron. Stud. **29**, 2383, **2020**.
35. MUSHTAQ M., TAN I., SAGIR M., TAHIR M.S., PERVAIZ M. A novel hybrid catalyst for the esterification of high FFA in Jatropha oil for biodiesel production. Grasasyaceites, **67**, 150, **2016**.
36. DUTTA B., KAR E., BOSE N., MUKHERJEE S. Significant enhancement of the electroactive β-phase of PVDF by incorporating hydrothermally synthesized copper oxide nanoparticles. RCS Advances, **5**, 105422, **2015**.
37. HENGLEIN A. Formation and absorption spectrum of copper nanoparticles from the radiolytic reduction of $Cu(CN)^{-2}$. The J. Phys. Chem. B, **104**, 1206, **2000**.
38. LI Y., WANG J.G., HUA W., LIU H., WEI B. Heterostructured Sn/SnO_2 nanotube peapods with a strong plasmonic effect for photoelectrochemical water oxidation. J. Mater. Chem. A. **7**, 16883, **2019**.
39. DIECKMANN Y., CÖLFEN H., HOFMANN H., PETRI-FINK A. Particle size distribution measurements of manganese-doped ZnS nanoparticles. Anal. Chem. **81**, 3889, **2009**.
40. WANG Y., NIU C., WANG D. Metallic nanocatalysts for electrochemical CO_2 reduction in aqueous solutions. J. Colloid Interf. Sci. **527**, 95, **2018**.
41. WANG J., JI Y., SHAO Q., YIN R., GUO J., LI Y., HUANG X. Phase and structure modulating of bimetallic CuSn nanowires boosts electrocatalytic conversion of CO_2. Nano Energy, **59**, 138, **2019**.
42. WANG J., ZOU J., HU X., NING S., WANG X., KANG X., CHEN S. Heterostructured intermetallic CuSn catalysts: high performance towards the electrochemical reduction of CO_2 to formate. J. Mater. Chem. A. **7**, 27514, **2019**.
43. SEN S., LIU D., PALMORE G. Electrochemical reduction of CO_2 at copper nanofoams. Acs Catalysis, **4**, 3091, **2014**.
44. QIAO J., JIANG P., LIU J., ZHANG J. Formation of Cu nanostructured electrode surfaces by an annealing-electroreduction procedure to achieve high-efficiency CO_2 electroreduction. Electrochem. Commun. **38**, 8, **2014**.
45. KUMAR B., ATLA V., BRIAN J.P., KUMARI S., NGUYEN T.Q., SUNKARA M., SPURGEON J.M. Reduced SnO_2 porous nanowires with a high density of grain boundaries as catalysts for efficient electrochemical CO_2- into- HCOOH conversion. Angewandte Chemie Int. Edit. **56**, 3645, **2017**.
46. DU D., LAN R., HUMPHREYS J., SENGODAN S., XIE K., WANG H., TAO S. Achieving both high selectivity and current density for CO_2 reduction to formate on nanoporous tin foam electrocatalysts. Chem. Select. **1**, 1711, **2016**.